Iraqi Journal of Oil & Gas Research

Journal homepage: https://ijogr.uotechnology.edu.iq/

Crack Growth in AL 6061-T6 in Thin Plates Used in Petroleum Equipment Under Dynamic Load

[1]Azhar Sabah Ameed, [1]Farag Mahel Mohammed, [1]Ahlam Luaibi Shuraiji*

[1] University of Technology/ Electromechanical Department, Baghdad-Iraq, Baghdad-Iraq

Article information

Article history:
Received: March, 20, 2024
Revised: April, 30, 2024
Accepted: May, 04, 2024
Available online: October, 04, 2024

Keywords:
Dynamic load,
Crack growth
Crack length,
Impact load.

Corresponding Author:
Azhar Sabah Ameed
50085@uotechnology.edu.iq

Abstract

Studying crack growth in aluminium alloys helps design safer structures and components. It allows more durable and flexible products to develop, resulting in enhanced safety and performance. Cracks in oil and gas equipment can cause accidents and environmental damage. The study investigated the influence of the dynamic load of a 6061-T6 aluminium plate with two fixed edges with dimensions of 80 mm and two free edges at variable dimensions of 80 mm, and 160 mm. A crack was created in the middle of an aluminium plate using a laser beam of thickness 0.08mm. The crack had different lengths, 3mm, and 5mm, and was created at angles of 0, 45, and 90 degrees. The study focused on determining the initial crack growth caused by the dynamic impact load caused by the free fall weight at a rate of 20 impacts per minute, the study performed experimental, numerical, and analytical investigations. Based on the experimental results, it was observed that increasing the crack length from 3 mm to 5 mm reduced the initial growth time by 45% in a plate with an aspect ratio of 1:1. However, in a plate with an aspect ratio of 1:2, the percentage of reduction in initial growth time was 16.5%. The results showed that increasing the crack angle from 0 to 90 degrees prolonged the crack growth in all samples with the same test conditions. The study's significance lies in determining the time required for crack growth in thin plates of this commonly used alloy in oil and gas applications like liquefied natural gas storage tanks, pipes, tanks, drilling equipment, and cutters. The research outcomes will provide valuable insights into the material's behavior, contributing to developing improved products and processes in this sector.

DOI: http://doi.org/10.55699/ijogr.2024.0402.1067 , Department of Oil and Gas Engineering, University of Technology-Iraq

1. Introduction

Cracks in oil and gas equipment can cause accidents and environmental, and human damage. A crack study is essential to prevent this by improving reliability, preventing costly repairs, saving money, ensuring regulatory compliance, improving performance, and reducing the risk of crack formation. Stress distribution is the way stress spreads across a material or structure under external loads. It depends on factors such as the structure geometry, material properties, and type of loading. Deformation is caused by internal forces or stresses that can cause cracks. Cracks can increase stress distribution and lead to further crack propagation, ultimately leading to component failure or breakage. The main objective of the study was to gather the most recent findings on numerical methods used to simulate fracture problems, which is a rapidly evolving area of research [1-3]. The study investigated the impact of stress on a large-scale oil tank with a floating roof. Specifically, the study focuses on the high-stress levels on the fillet joint and analyzes how three key tank parameters affect it. The study proposes a new method to enhance the design of large-scale oil tanks and evaluate their structural integrity [4]. Oil storage tanks are crucial in the petroleum industry but are prone to damage. To ensure their service life and prevent environmental disasters, this study covers common defects, design, construction, repair standards, and methods to prevent crack growth. The study uses techniques like finite element simulation and the design of experiments to assess the tank structure in different modes and analyze the effects of geometric parameters of defects [5]. The study investigates the behavior of a cracked aluminum pipe repaired with a glass/epoxy composite patch under fatigue tension loading. The numerical model includes deboning the adhesive layer between the pipe and the composite patch and crack growth in the aluminum pipe. The study considers three different shapes of composite patches and a parametric study to observe the effect of fiber orientation on fatigue crack growth. These findings could lead to optimized designs of patch-repaired pipes under fatigue loading [6]. Aluminum alloy is commonly used for LNG storage systems. To predict its service life, researchers assess its mechanical properties, such as tensile strength, fatigue performance, and fracture toughness. A new model was suggested in this study to consider the mean stress effect on the fatigue crack growth rate (FCGR) of aluminum alloy in a unified manner. The model was validated by comparing FCGR test data of aluminum alloy with Walker's relationship. The new model showed more accurate results compared to the Walker model [7]. The study explores the relationship between detonation load and crack propagation in pipes. A material model combined with a fluid-structure coupling approach was used to simulate the dynamic fracture of aluminum pipes due to internal gaseous detonation. The study identified the factors affecting crack propagation and proposed a formula to calculate the oscillating frequencies of crack speeds. The results can be useful for investigating pipe explosion accidents [8]. Transportation of liquefied gas cargo on a small scale has been growing, and Type C containment systems offer a potential solution. These systems, which feature end saddle supports, are frequently used for short- to medium-distance transportation. To accommodate thermal contraction and expansion resulting from temperature changes, one end is fixed while the other is meant to slide. Type C cargo/fuel tanks, known as "pressure vessels," are designed to meet recognized standards and codes like ASME BPVC. These tanks do not need to maintain the hull strength or integrity of the vessel but should endure all static and dynamic loads during their service life. There are two categories of Type C tanks used in liquefied gas cargo vessels or gas-fueled ships: foam-insulated single-shell tanks [9]. Analyses were conducted on the fatigue fracture propagation rates in thick aluminum alloy 5083-0 plates intended for use in LNG tanks. The rates at room temperature and at -320°F were determined. The growth of welds was compared to the growth of the parent material. The rates of surface flaw growth under tension and combined tension/bending were established. Additionally, the rates of surface flaw growth under spectrum loading were compared with calculated rates from constant amplitude loading data [10]. The PAW on cryogenic materials for LNG fuel tanks was assessed in this work. It evaluated fracture and weld joint fatigue at various temperatures. Material kinds and PAW parameters were investigated. The findings advise taking PAW into account when designing LNG tanks [11]. With an emphasis on LNG fuel tank construction, they investigated welding techniques and the fracture toughness of 9% nickel steel. They looked at how groove angle affected the morphology of the weld, contrasted FCAW with laser beam welding at cryogenic temperatures, and investigated fatigue in joints made of Invar alloy and SUS 304L [12-16]. This study offers a streamlined method for evaluating pressure vessel leak-before-break or failure. It draws attention to the prospect of stopping vessel failure by identifying stable through-thickness cracks that are leaking early on. This method is validated using available test data [17]. Crack propagation in a spherical LNG tank is crucial for safety. Different fatigue crack growth models are used for analysis, considering stress ratios and past load history effects. Evaluating crack growth under various operating conditions and stress sequences helps in

studying these effects [18]. When standards are broken, cargo ships may sustain unanticipated loads that cause structural damage. To improve reliability, stress monitoring systems are incorporated in strategic locations. To improve operating safety, a study integrated stress data from hull strain sensors with fatigue analysis to predict residual fatigue life in real time [19]. The present study aims to determine the time required for crack propagation in the Al 6061-T6 thin plate under dynamic loading. This alloy is widely used in various applications of the oil and gas industry, such as storage tanks for liquefied natural gas (LNG), pipes, tanks, drilling equipment, and cutters. The research outcomes are expected to provide valuable insights into the behavior of this material, which will be instrumental in developing improved products and processes in this sector.

2. Theoretical Part

Certain assumptions were made to derive the equations for plate theory and solve it. These assumptions are:

1. The plate material is linearly elastic and follows Hooke's law.
2. The plate is homogeneous and isotropic.
3. The impact load is applied perpendicularly to the middle plane of the plate

2.1 The impact-loading force

Using the work-energy principle [20], the impactor's velocity can be described as follows:

$$PE = KE \tag{1}$$

Where PE is a potential energy and KE is a kinetic energy.

$$mgH = \frac{1}{2}\, m\, V^2 \tag{2}$$

Where, m is impactor mass (kg), g is gravitational acceleration (m/sec^2), H height of impactor and V is the velocity of impactor (m/sec)

$$V = \sqrt{2gH} \tag{3}$$

Using the work-energy (We) principle from initial velocity V_{intial} and final velocity V_{final}:

$$\mathrm{We} = \frac{1}{2}mV_{final}^2 - \frac{1}{2}mV_{inital}^2 \tag{4}$$

$$V_{inital} = 0 \ , \ V_{final} = V \tag{5}$$

$$\mathrm{We} = \frac{1}{2}mV^2 \tag{6}$$

From equation (6) the force of impact loading [21]:

$$F_{impct} = 2\mathrm{We}/\mathrm{H} \tag{7}$$

2.2 The impact loading force with time relation

Assume, as shown in Figure 1, that the impactor moves down from its position inside the device to impact the plate surface with a force equal to F_{impct}. It then takes T time to return to its original state.

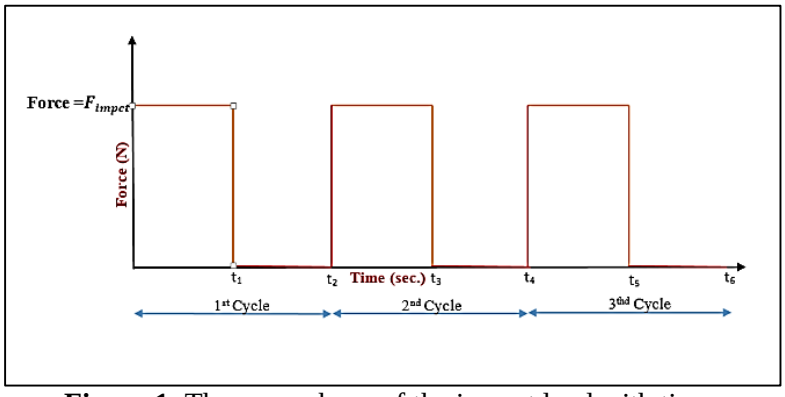

Figure 1: The wave shape of the impact load with time.

In order to solve the problem of representing periodic functions effectively, a mathematical model utilizing the Fourier series method was employed [22].

$$F(x.y.t_i) = \frac{a_o}{2} + \sum_{n=1}^{N}\left[a_n \cos\left(\frac{n\pi t}{L}\right) + b_n \sin\left(\frac{n\pi t}{L}\right)\right] \quad (8)$$

Where: a_o, a_n, and bn are periodic function over (–L, L), L is one period time Cycling force of impact loading for one periodic, as a function of time (t) in (sec).

$$F(x.y.t_i) = \begin{cases} F_{impct} & 0 \le t \le t_1 \\ 0 & t_1 < t \le t_2 \end{cases} \quad (9)$$

To generate the final equation (10), Equation (9) can be written by substituting estimated values of ao, an, and bn in Equation (8)

$$F(x.y.t_i) = \frac{1}{2L}\int_{-L}^{L} T.dt + \sum_{n=1}^{N}\left[\begin{array}{l} \frac{1}{L}\int_{-L}^{L} T\cos\left(\frac{n\pi t}{L}\right)dt \cos\left(\frac{n\pi t}{L}\right) + \\ \frac{1}{L}\int_{-L}^{L} T\sin\left(\frac{n\pi t}{L}\right)dt \sin\left(\frac{n\pi t}{L}\right) \end{array}\right] \quad (10)$$

2.3 The governing equation

The equation for calculating deflection in Cartesian coordinates takes into account the impact load F. Levy's solution provides formulas for plates that are clamped on both ends or simply supported on one side and free on the other. These formulas are used to determine the governing equation for plates under impact load [23].

$$D\left(\frac{\partial^4 w}{\partial x^4} + 2\frac{\partial^4 w}{\partial x^2\,\partial y^2} + \frac{\partial^4 w}{\partial y^4}\right) + m_2\frac{\partial^2 w}{\partial t^2} = F(x.y.t_i) \quad (11)$$

Where:-

$$D = \frac{E_2 h^3}{12(1-\nu_2^2)} \quad (12)$$

D is cylindrical rigidity of plate, h plate thickness, E2, υ2 are the young's modules and Poisson's ratio of plate respectively.

The initial condition of the problem are:-

w = 0 and $\frac{\partial w}{\partial t} = 0$ at t = 0

By the initial condition the will get equation:

$$\frac{\partial^4 w}{\partial x^4} + 2\frac{\partial^4 w}{\partial x^2\,\partial y^2} + \frac{\partial^4 w}{\partial y^4} = \frac{F(x.y.t_i)}{D} \quad (13)$$

The total solution for deflection w includes both the homogeneous solution for deflection, represented by w_h, and the particular solution for deflection, represented by w_p [24]:-

$$w = w_h + w_p \quad (14)$$

The general solution by using initial condition will be:

$$w = \sum_{m}^{\infty}\left[\frac{F(t_i)A^4}{\pi^4 m^4 D} + C_2\cosh\alpha_m y + \alpha_m y(C_3\sinh\alpha_m y)\right]\sin\alpha_m x \quad (15)$$

2.4 Boundary Conditions

In Figure 2, the plate dimensions are displayed along with the axes' directions and the boundary conditions for the plate with crack orientation. Consider a plate that has its edges clamped at x = 0 and x = A, while being free supported at the opposite edges y = 0 and y = B [25].

At: y = B/2 at x = 0 and x = A, w = 0

$$\frac{F(t_i)A^4}{\pi^4 m^4 D} + C_2\cosh\beta_m + C_3\beta_m\sinh\beta_m = 0 \quad (16)$$

Where: $\beta_m = \frac{m.\pi.B}{2A}$, At: $y = \frac{B}{2}$ at $x = 0$ or $x = A$. $\frac{\partial w}{\partial y} = 0$

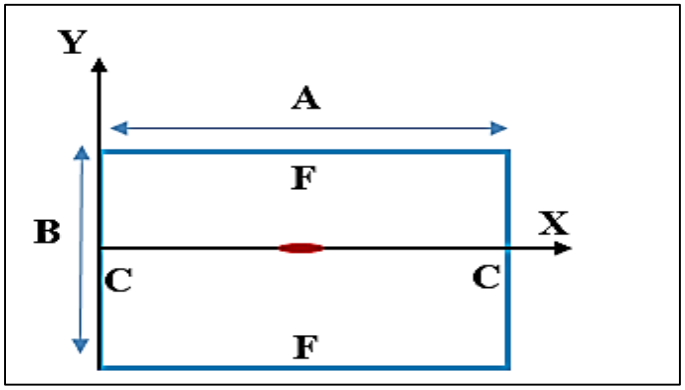

Figure 2: The clamped type of plate is CFCF.

$$C_2\sinh\beta_m+C_3(\beta_m.\cosh\beta_m+\sinh\beta_m)=0 \quad (17)$$

From equations 16 and 17 get:

$$C_2 = \frac{-F(t_i)A^4}{\pi^4 m^4 D}\cdot\frac{(1+\beta_m\coth\beta_m)}{\beta_m\,\mathrm{csch}\,\beta_m+\cosh\beta_m} \quad (18)$$

$$C_3 = \frac{F(t_i)A^4}{\pi^4 m^4 D}\cdot\frac{1}{\beta_m\,\mathrm{csch}\,\beta_m+\cosh\beta_m} \quad (19)$$

A MATLAB 17 program was used to confirm the accuracy of the mathematical analysis.

3. Experimental Procedure

3.1 Material And Methods

The study relied on the use of a 6061-T6 aluminum plate with a thickness of 2 mm, which was cut into dimensions of 80 mm by 80 mm, 80, and 80 mm by 160 mm. The crack was created with a thickness of 0.08 mm and a length of 3 mm and 5 mm using a CNC fiber laser machine, as shown in Figure 3. The study adopted a digital crack length measuring device type CK102 to measure the crack width and change in the length of the crack with time under dynamic shock load as shown in Figures 4-a and b. Table 1 shows the chemical composition of 6061-T6 aluminum alloy, while Table 2 shows its mechanical properties. The dynamic impact device was designed and manufactured for an aluminum plate fixed by two edges with dimensions of 80 mm by 80 mm and free from the other two edges of variable dimensions (Clamped -Free -Clamped- Free) CFCF. The impactor weight was 1.5 kg, with 20 impacts per minute. The electromechanical device shown in Figure 5 includes the ability to determine the number of impacts per minute through a control board that controls the rotation speed of the electric motor with a sensor to indicate the completion of one revolution.

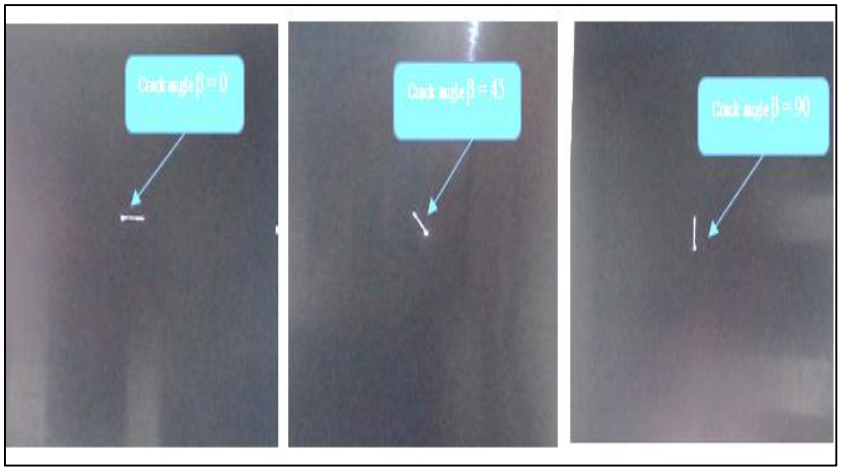

Figure 3: Plates crack angle.

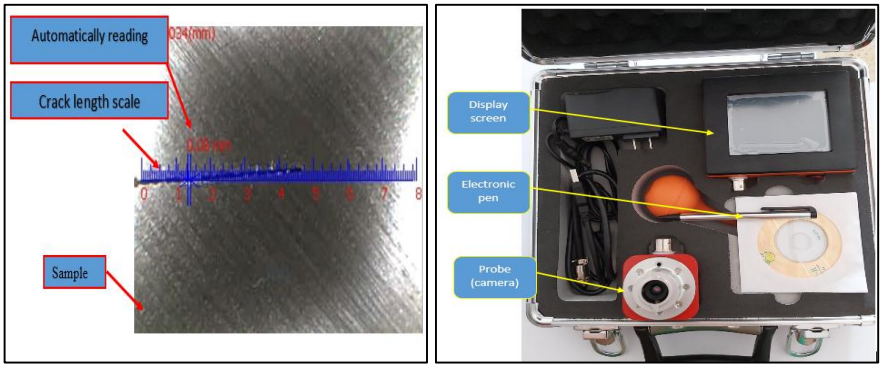

a) Digital measuring the crack length **b)** The components of CK102 device

Figure 4-a, and b: The digital CK102 device of measuring crack length.

Table 1: Chemical composition of Aluminum alloy 6061-T6.

Si%	Fe%	Cu%	Mn %	Mg%	Cr%	Zn%	Ti%	Other elements
0.74	0.42	0.22	0.07	1.04	0.12	0.04	0.04	0.1

Table 2: Mechanical properties of Aluminum alloy 6061-T6.

Elastic modulus (GPa)	Passion ratio	Ultimate tensile strengths MPa	Tensile yield strengths (MPa)
68.9	0.33	310	276

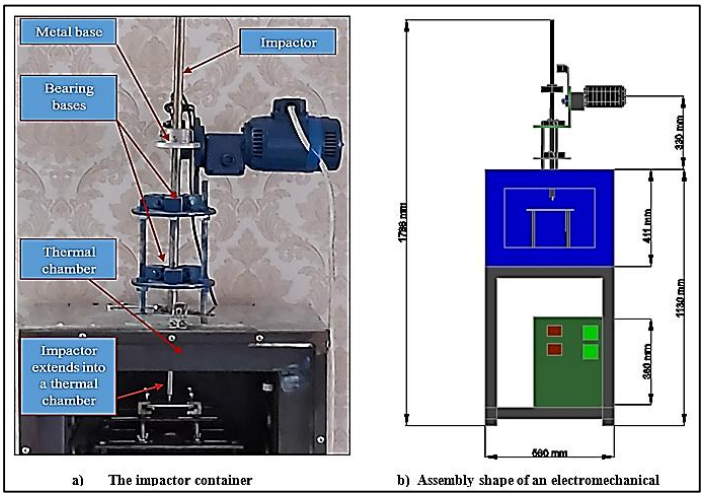

Figure 5-a, and b: The impactor electromechanical device**.**

4. Numerical analysis

4.1 Three-dimensional fracture modeling

By using quadratic elements, a three-dimensional model 3D was created to analyze a plate with a central crack. The mechanical and thermal properties of the plate's material, as well as the stresses caused by the impact load, were defined, to determine the impact area and establish all the necessary initial conditions such as the plate's dimensions, crack length, crack angle, and installation method. As shown in Figures 6 and 7.

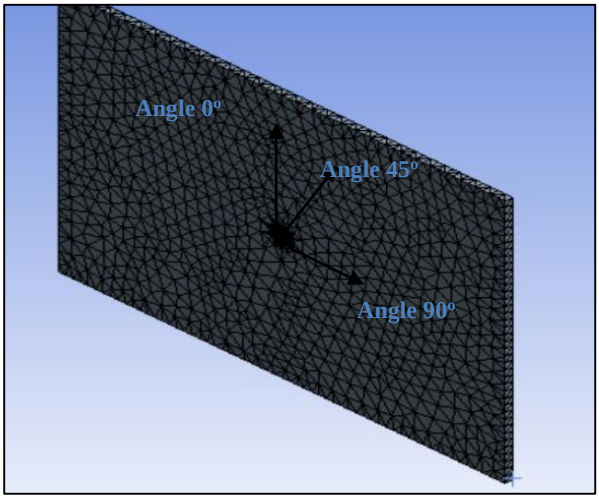

Figure 6: 3D meshing elements for plate and crack angle.

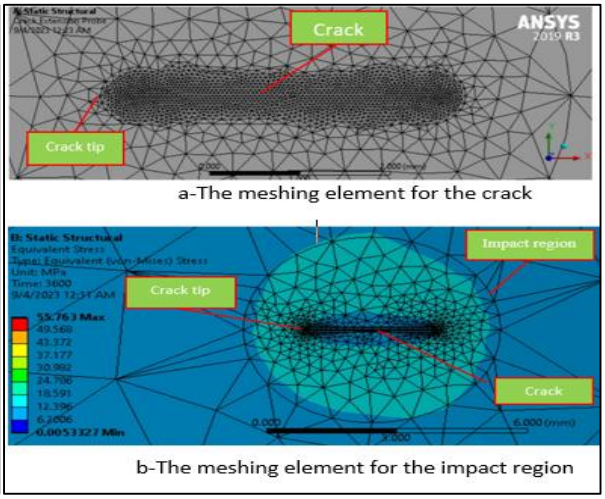

Figure 7: 3D meshing elements for crack.

4.2 Boundary conditions

4.2.1 Apply impact stress

The purpose of building the model by using Ansys software is to analyze the force of impact on the sample surface based on the electromechanical device's impact specifications, such as the weight of the impactor, the distance between the impactor, the thin plate of Al6061-T6, and the diameter of the impactor. The model simulated the impact stress caused by the force of the impactor on the plate. The contact surface area between the impactor and the plate was defined, and the impactor was accurately configured with all its necessary data and the applied load function as shown in Figure 8. The outputs of maximum stress on three axes obtained from the first model (impact model) were then used as inputs for the second model to simulate the crack growth.

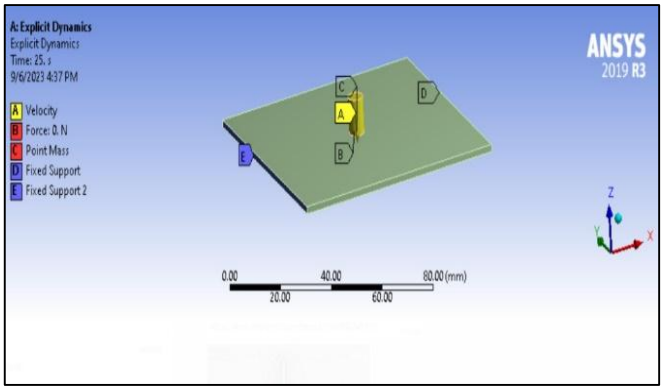

Figure 8: Impact specifications.

4.2.2 Sample fixation method

The study examined fixation techniques clamped-clamped with free at the other edges of plate CFCF, for all sample types as shown in Figure 9.

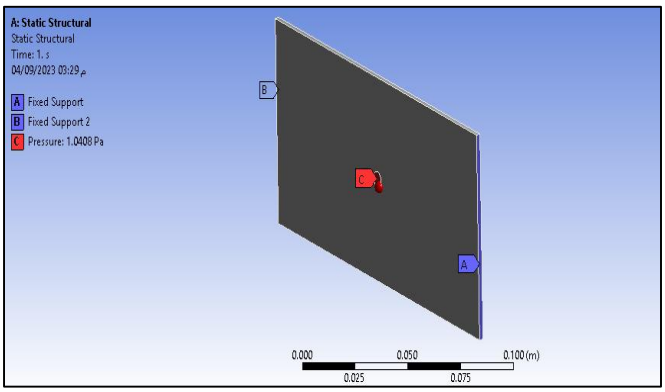

Figure 9: The plate CFCF.

4.3 Smart crack growth

At each solution step, SMART automatically updates the mesh of crack geometry that changes due to crack growth. This is different from the extended finite element method (XFEM), which relies on the use of an enrichment (segmentation) region. Figure 10 shows the final model built using SMART to calculate the growth of the crack after constructing models based on the output of the first model (impact model).

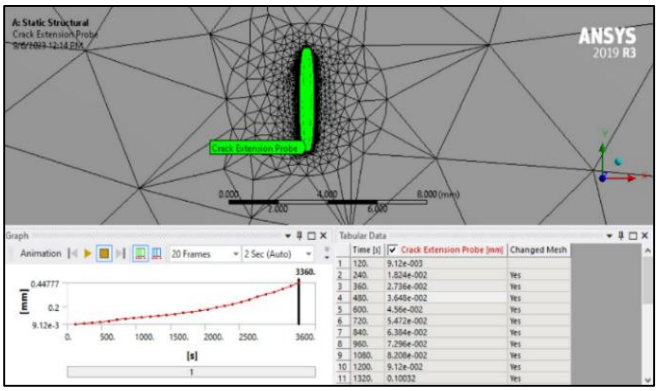

Figure 10: Smart crack growth.

5. Results and Discussion

5.1 The effect of crack angle

Figure 11 illustrates the propagation of cracks in A-80-3-0-CFCF with an aspect ratio of 1:1. The time required for crack propagation, (Tp), has been estimated through analytical, numerical, and experimental methods. The analytical results suggest that Tp is approximately 166,000 seconds, and the number of impacts needed to initiate crack propagation is estimated at 55,333. Similarly, numerical results indicate that the crack growth started at Tp of 166,840 seconds, and approximately NipN was 55,613 impacts. The experimental estimation revealed that crack growth started at Tp around 166,960 seconds, after 55,653 impacts. The overall relative difference between the analytical and experimental results was about 5% in the estimated values of Tp and Nip, and about 2.7% between the numerical and experimental of Tp and Nip. When the angle of the crack was changed from 0° to 45°, as depicted in Figure 12, the crack began to grow after approximately 175,300 seconds and with a NipA of 58,433 impacts, according to the analytical results. The numerical results estimated that the crack started to propagate after 175,474 seconds, with a NipN of 58,491 impacts. In the experimental results, it was observed that the crack required 175,600 seconds and 58,533 impacts to initiate growth. Increasing the crack angle from 0° to 45° led to a 5% increase in the values of Tp and Nip. However, when the crack angle was 90° under the same test conditions and for the same specimen shown in Figure 13, it required a 7% increase in the values of Tp and Nip. When comparing Tp and Nip for a CFCF with a crack length of 3 mm as shown in Figures 11 to 13, it was observed analytically, numerically, and experimentally that the mechanical behavior of the crack propagation was notably affected by the angle of the crack. The crack at the 0° angle required the least Tp and Nip compared to other angles because the direction of the crack length was towards the y-axis. This generated high stresses in the 0° crack direction and caused tensile stresses that had the greatest effect on crack growth. As the angle increased

from 0° to 45°, the stress components decayed, and the horizontal components of mechanical stress were eliminated, resulting in less effect on the crack propagation. At an angle of 90°, compressive stresses were exerted on the crack, which helped restrict the growth and spread of the crack. This is due to the Fixation technique CFCF, in which the fixed edge was in the same direction as the 90° angle. Even when the aspect ratio is 1:2, the above observations apply, which are demonstrated in Figures 14. When testing samples with a crack length of 5mm under the same experimental conditions, the crack angle's effect on the growth rate remained notable, where the highest growth rate was observed when the angle was 0, and it decreased as the angle increased, regardless of the plates aspect ratio. Figures 15 to 17 display crack propagation in samples with a 5 mm crack length, at varying crack angles and aspect ratios. Tables 3 and 4 display the percentage increase in the number of impacts required for the crack to start propagation analytically NipA, numerically NipN, and experimentally NipE, resulting from a change in crack angle. Results were in good agreement with Khan, et al. [26] and Pook, L. P.z [27].

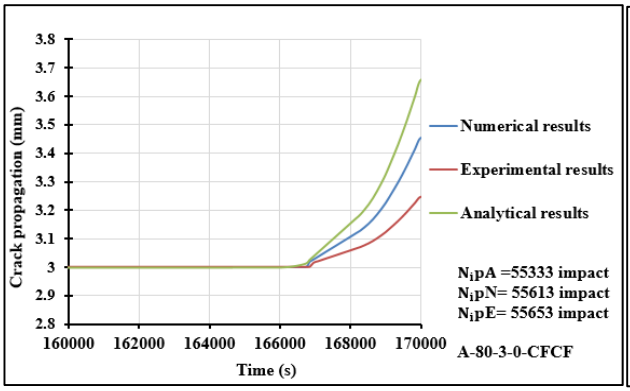

Figure 11: Crack propagation with time for A-80-3-0-CFCF.

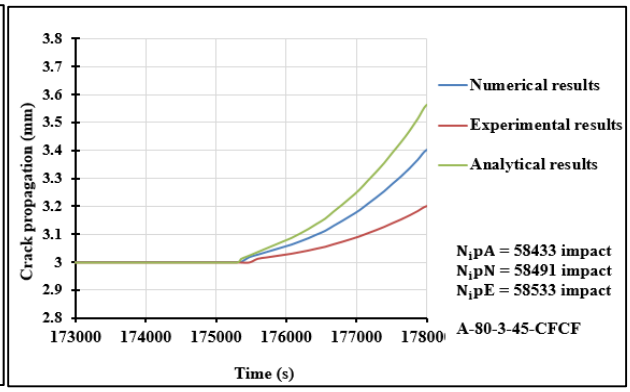

Figure 12: Crack propagation with time for A-80-3-45-CFCF.

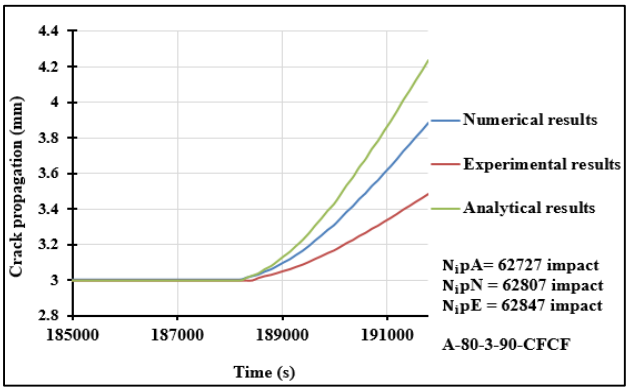

Figure 13: Crack propagation with time for A-80-3-90-CFCF.

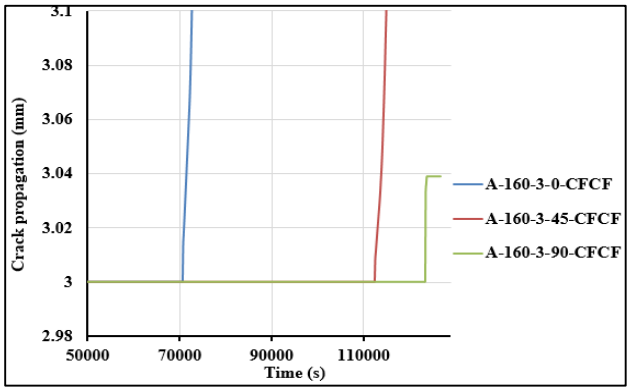

Figure 14: Crack propagation with time estimated experimentally for A-160-3-(0,45,90)-CFCF.

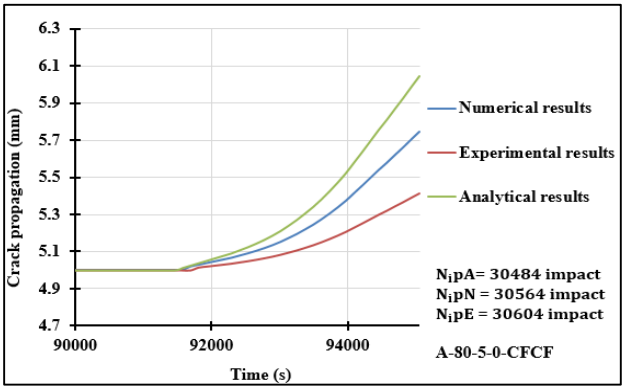

Figure 15: The crack propagation with for A-80-5-0-CFCF.

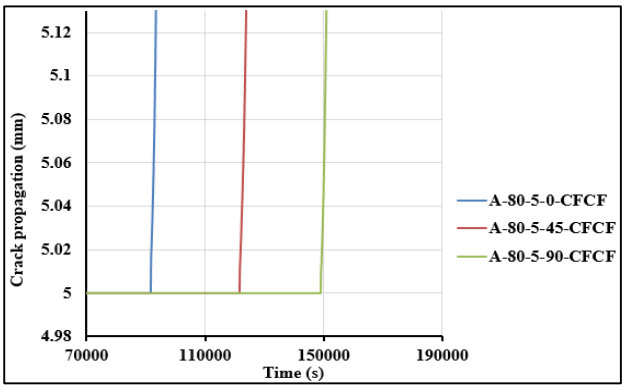

Figure 16: Crack propagation with time estimated experimentally for A-80-5-(0,45, 90)-CFCF.

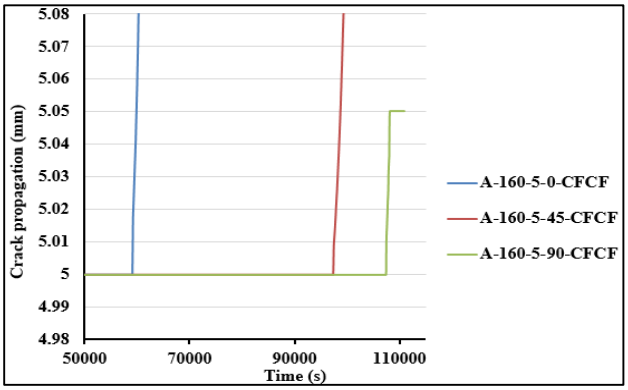

Figure 17: Crack propagation with time estimated experimentally for A-160-5-(0,45, 90)-CFCF.

Table 3: Percentage increase in Nip, resulting from a change in crack angle, with a crack length of 3mm

Specimen Type	Impact number (Nip)	The percentage increase in Nip from 0° to 45°	The percentage increase in Nip from 45° to 90°	The percentage increase in Nip from 0° to 90°
(80*80)	NipA	5%	7%	12%
	NipN	5%	7%	11%
	NipE	5%	7%	11%
(80*160)	NipA	37%	9%	43%
	NipN	37%	9%	43%
	NipE	37%	9%	43%

Table 4: Percentage increase in Nip, resulting from a change in crack angle, with a crack length of 5mm

Specimen Type	Impact number (Nip)	The percentage increase in Nip from 0° to 45°	The percentage increase in Nip from 45° to 90°	The percentage increase in Nip from 0° to 90°
(80*80)	NipA	25%	18%	38%
	NipN	25%	18%	38%
	NipE	25%	18%	38%
(80*160)	NipA	39%	104%	45%
	NipN	39%	94%	45%
	NipE	39%	94%	45%

5.2 The effect of crack length

Table 5 shows the percentage increase in Tp required for crack propagation, analytically, numerically, and experimentally, resulting from the change in crack length from 5mm to 3mm. When the crack is exposed to a cyclic impact load, it opens and closes as a result of the stresses generated by this load. The effect of these stresses increases as the length of the crack increases, which leads to a higher concentration of energy in the crack tip, which leads to its growth faster than shorter cracks. In addition, when a material contains longer cracks, the plastic areas at the edges of those cracks become larger, causing plastic deformation. This deformation can facilitate the propagation of cracks, as the environment surrounding the cracks becomes more favorable for their growth. As the cracks become longer, the plastic area also increases, causing the cracks to propagate faster. Results were in good agreement with Ahmed, et al. [28].

Table 5: Percentage increase in Tp, resulting from a change in crack length from (5 to 3) mm estimated for 6061-T6 alloy, CFCF without thermal effect.

Specimen type	Crack angle	Analytically Tp %	Numerically Tp%	Experimentally Tp%
(80*80)	0^0	44.9%	45.0%	45.0%
	45^0	30.7%	30.7%	30.6%
	90^0	21.0%	21.0%	21.0%
(80*160)	0^0	16.6%	16.6%	16.5%
	45^0	13.4%	13.4%	13.4%
	90^0	12.9%	12.9%	13.0%

5.3. The effect of plate aspect ratio

In the experiments conducted, it was observed that the crack propagation of A-80-3-0-CFCF with an aspect ratio of 1:1, as shown in Figure 11, started growing at Tp around 166960 seconds. The crack growth in A-160-3-0-CFCF sample, on the other hand, started at Tp and Nip values which were approximately 57.5% lower than the previous sample, as shown in Figure 14. In Figure 13, when the crack angle was changed to 90 degrees in sample A-80-3-90-CFCF while the aspect ratio remained the same (1:1), the crack needed to start growing to Tp and Nip values that were approximately 34.5% higher than for sample A-160-3-90-CFCF shown in Figure 14.

Similarly, sample A-80-5-0-CFCF shown in Figure 15 had an aspect ratio of 1:1 required approximately 35.5% more values of Tp and Nip compared to the sample A-160-5-0-CFCF with an aspect ratio of 1:2 shown in Figure 17, when tested under the same conditions. As a plate's aspect ratio (A.R) increases, so does the stress, resulting in an increase in deflection and bending value. This means that deflection is directly proportional to stress. Therefore, dynamic crack propagation is more likely in plates with the highest aspect ratios. The results of the study confirmed this hypothesis, as the Tp and Nip values were lower in an aspect ratio of 1:2 compared to 1:1 under the same conditions.

5.4 Crack closure

In Figure 14, it is shown that the crack in the A-160-3-90-CFCF sample begins to grow at Tp around 123500 sec, as per experimental results, and stops at Tp 123620 sec. Similarly, in the case of sample A-160-5-90-CFCF, where crack growth starts at Tp around 107459 sec and stops at 108140 sec based on experimental tests.

It is clear that the crack gradually expanded and ultimately ceased propagation due to the crack closing. All cases were in an aspect ratio of 1:2 specimens with a 90° crack angle where the direction of the crack was towards the fixation side, which provided conditions for closing the crack because this phenomenon is affected by the fixation method and the dimensions of the specimen [30]. Additionally, crack closure occurs due to roughness-induced closure, which occurs due to mode II or in-plane shear loading. This is due to the mismatch of the rough fracture surfaces of the upper and lower parts of the crack. When mode II loading is applied, the heterogeneity in the microstructure leads to local out-of-plane deformation. As a result, the mismatched wedges come into contact during the cyclic impact loading process, resulting in the cracks closing. Misalignment of the fracture surfaces also occurs in the distal field of the fracture, which can be explained by asymmetric displacement and rotation of the material [29-31].

6. Conclusions

Through the experimental, numerical, and analytical results of Al-6061-T6 aluminum plate fixed from two edges with a dimension of 80 mm and free from the other two edges with different dimensions, which contain a crack of length 3 mm and 5 mm. The study aimed to determine the time required for crack propagation in 6061-T6 alloy under dynamic impact load. This alloy is commonly used for structural components, oil pipes, tanks, drilling equipment, and cutters. The study concluded the following:

- At a crack length of 3 mm and an inclination angle of 0 degrees, the time required for initial crack growth in an 80 mm by 80 mm plate was 57.5% longer than needed for a crack to grow in an 80 mm by 160 mm plate.In a plate measuring 80 mm by 80 mm with a crack length of 5 mm, the interval of time needed for a crack to grow at a 0^o angle of inclination is 35.5% larger than a plate measuring 80 mm by 160 mm.
- The change in the resulting crack length from 3 mm to 5 mm at a 0 degree angle in the plate with dimensions 80 mm by 80 mm results in a decrease in the time required for initial crack growth by 45%, while the reduction in time was 16.5% in the plate 80 mm by 160 mm. The experimental results revealed that the change in the angle of crack inclination at a crack length of 3 mm, from 0 to 45, the ratio of increase in the time of initial crack growth in a plate measuring 80 mm by 80 mm was 5%. However, the increasing ratio in the plate measuring 80 mm by 160 mm was 37.5%.
- The experimental results show that the change in the angle of crack inclination at a crack length of 3 mm, from 45 to 90 degrees, in a plate with dimensions 80 mm by 80 mm due to an increase in the time of creating the increased initial crack by the ratio of 7 %. However, the ratio of increase in the plate measuring 80 mm by 160 mm was 9 %.

Nomenclature

NipN	The number of impacts required for the crack to start propagation numerically
NipE	The number of impacts required for the crack to start propagation experimentally
NipA	The number of impacts required for the crack to start propagation analytically
80-3-0-CFCF	The specimen with dimensions 80 mm by 80mm has a crack 3 mm with angle 0^o fixed from two edges
160-3-0-CFCF	The specimen with dimensions 160 mm by 80mm has a crack 3 mm with angle 0^o fixed from two edges
80-5-0-CFCF	The specimen with dimensions 80 mm by 80mm has a crack 5 mm with angle 0^o fixed from two edges
160-5-0-CFCF	The specimen with dimensions 160 mm by 80mm has a crack 5 mm with angle 0^o fixed from two edges
80-3-45-CFCF	The specimen with dimensions 80 mm by 80mm has a crack 3 mm with angle 45^o fixed from two edges
160-3-45-CFCF	The specimen with dimensions 160 mm by 80mm has a crack 3 mm with angle 45^o fixed from two edges
80-5-90-CFCF	The specimen with dimensions 80 mm by 80mm has a crack 5 mm with angle 90^o fixed from two edges
160-5-90-CFCF	The specimen with dimensions 160 mm by 80mm has a crack 5 mm with angle 90^o fixed from two edges

Acknowledgements

We would like to thank the University of Technology, especially the Electromechanical Department and Center of Training and Factory for their support in completing this work.

References

[1] Giannella, V.; Sepe, R.; Citarella, R. Fatigue crack propagation for an aircraft compressor under input data variability. Procedia Struct. Integr. 2022, 41, 298–304.

[2] Giannella, V. Uncertainty quantification in fatigue crack-growth predictions. Int. J. Fract. 2022, 235, 179–195.

[3] M. Hagarová, G. Baranová, P. Peterka, B. Buľko, M. Hrubovčáková, and V. Girman, "Failure analysis of a gas pipeline at the kinked dent location with crack indications," Eng. Fail. Anal., vol. 153, p. 107579, Nov. 2023.

[4] L. Shi, J. Shuai, X. Wang, and K. Xu, "Experimental and numerical investigation of stress in a large-scale steel tank with a floating roof," Thin-Walled Struct., vol. 117, pp. 25–34, Aug. 2017.

[5] K. Reza Kashyzadeh, M. Omidi Bidgoli, S. S. Rahimian Koloor, and M. Petrů, "Assessment of oil storage tanks performance containing cracks and cavities," Above Gr. Storage Tank Oil Spills Appl. Case Stud., pp. 3–42, Jan. 2022.

[6] H. Zarrinzadeh, M. Z. Kabir, and A. Deylami, "Crack growth and debonding analysis of an aluminum pipe repaired by composite patch under fatigue loading," Thin-Walled Struct., vol. 112, pp. 140–148, Mar. 2017.

[7] Y. Choi, D.-G. Kim, J.-Y. Park, K.-S. Lee, J.-M. Lee, and M.-H. Kim, "An Experimental Investigation about Fatigue Crack Growth Rate of Aluminum Alloy Considering Various Mean Stress." May 31, 2015.

[8] Y. Du, F. Zhou, W. Hu, L. Zheng, L. Ma, and J. Zheng, "Incremental dynamic crack propagation of pipe subjected to internal gaseous detonation," Int. J. Impact Eng., vol. 142, p. 103580, Aug. 2020.

[9] Guidance Notes on Strength Assessment of Independent Type C Tanks, American Bureau of Shipping Incorporated by Act of Legislature of the State of New York 1862, 2022 American Bureau of Shipping. All rights reserved. ABS Plaza 1701 City Plaza Drive Spring, TX 77389 USA.

[10] RA Kelsey , GE Nordmark , JW Clark, Fatigue Crack Growth in Aluminum Alloy 5083-0 Thick Plate and Welds for Liquefied Natural Gas Tanks, Publisher: ASTM International, Publication date:1974.

[11] Tae-Yeob Kim, Sung-Won Yoon, Ji-Hoon Kim and Myung-Hyun Kim, Fatigue and Fracture Behavior of Cryogenic Materials Applied to LNG Fuel Storage Tanks for Coastal Ships, Metals 2021, 11, 1899.

[12] Kim, B.E.; Park, J.Y.; Lee, J.S.; Lee, J.I.; Kim, M.H. Effects of the welding process and consumables on the fracture behavior of 9 wt.% nickel steel. Exp. Tech. 2019, 44, 175–186 .

[13] Kim, B.E.; Park, J.Y.; Lee, J.S.; Kim, M.H. Study on the Initial Design of an LNG Fuel Tank using 9 wt.% Nickel Steel for Ships and Performance Evaluation of the Welded Joint. J. Weld. Join. 2019, 37, 555–563.

[14] Kim, J.W.; Kim, J.S.; Kang, S.W.; Chun, K.S. Laser welding of ASTM A553-1 (9% Nickel Steel) (PART I: Penetration shape by bead on plate). Metals 2020, 10, 484.

[15] Kim, J.W.; Kim, J.S. Laser Welding of ASTM A553-1 (9% Nickel Steel) (PART II Comparison of Mechanical Properties with FCAW). Metals 2020, 10, 999.

[16] Oh, D.J.; Kim, N.K.; Song, S.W.; Kim, Y.D.; Kim, M.H. Investigation of fatigue performance for new membrane-type LNG CCS at cryogenic temperature. J. Marstruc. 2018, 62, 90–105.

[17] P. Kannan, K.S. Amirthagadeswaran, T. Christopher, B. Nageswara Rao , A simplified approach for assessing the leak-before-break for the flawed pressure vessels, Nuclear Engineering and Design, Volume 302, Part A, June 2016, Pages 20-26.

[18] Myung-Sup Lee and Myung-Hyun Kim, Fatigue Crack Growth Evaluation of IMO Type B Spherical LNG Cargo Tank Considering the Effect of Stress Ratio and Load History, Journal of Welding and Joining, Vol.40 No.1(2022) pp40-47.

[19] Seung Geon Leea, Young-Jun Yang , Won-Du Chang and Jung Min Sohn, Predicting the residual fatigue life of a cargo hull tank using a deep-learning technique, JOURNAL OF INTERNATIONAL MARITIME SAFETY, ENVIRONMENTAL AFFAIRS, AND SHIPPING 2020, VOL. 4, NO. 3, 84–92.

[20] Douglas W. MacDougal, Newton's Gravity: An Introductory Guide to the Mechanics of the Universe, 2012th ed. Springer.

[21] R. Metz, "Impact and drop testing with ICP force sensors," Sound Vib., vol. 41, no. 2, pp. 18–20, 2007.

[22] Hobson, Ernest (1911). "Fourier's Series". Encyclopædia Britannica. Vol. 10 (11th ed.). pp. 753–758.

[23] Loke Sworappa, and R. Dharni, "Laminated Architectural Glass Subjected to Blast, Impact Loading", International Journal of Impact Engineering December 2006.

[24] R. Szilard, Theories and Applications of Plate Analysis, Wiley, (2004)2004.

[25] Stephen P. Timoshenko, and S. Woinowsky-Krieger, "Theory of Plates and Shells", second edition, 1986.

[26] S. Khan, M. Junaid, and F. N. Khan, "Investigating the Effect of Crack's Inclination on Strain Energy and Stress Intensity under Uniaxial Loading †," Eng. Proc., vol. 23, no. 1, 2022.

[27] L. P. Pook, "The effect of crack angle on fracture toughness," Eng. Fract. Mech., vol. 3, no. 3, pp. 205–218, Oct. 1971, doi: 10.1016/0013-7944(71)90032-4.

[28] B. A. Ahmed and F. A. Alshamma, "Dynamic crack propagation in thin plates under cycling thermal stresses effect with cycling impact loading," J. Mech. Eng. Res. Dev., vol. 43, no. 7, pp. 1–11, 2020.

[29] Shouxin Li, Lizhi Sun, Qishan Zang, and Zhongguang Wang, "A geometric model for fatigue crack closure induced by fracture surface roughness under mode I displacements," 1992.

[30] R. O. Suresh, S.;Ritchie, "A Geometric Model For Fatigue Crack Closure Induced By Fracture Surface Roughness". LBL Publications Materials Sciences Permalink:, 1982.

[31] R. Pippan, G. Strobl, H. Kreuzer, and C. Motz, "Asymmetric crack wake plasticity – a reason for roughness induced crack closure", Acta Mater, vol. 52, no. 15, pp. 4493–4502, Sep. 2004.